Science of the Total Environment 1005 (2025) 180858

Contents lists available at ScienceDirect

Science of the Total Environment

journal homepage: www.elsevier.com/locate/scitotenv

# Newly discovered $CO_2$ (carbon dioxide) vent cave drives r-strategy shift in a Mediterranean aphotoendosymbiotic coral

Chiara Cassarino [a,1], Arianna Mancuso [a,b,1], Fiorella Prada [a,c], Teresa Sani [a,b,d], Silvia Dall'Ara [a], Oscar Wallnoefer [a], Chiara Marchini [a,b,i], Franco Tassi [e,f], Alessandra Campanelli [d], Mauro Marini [b,d], Jörg U. Hammel [g], Jaap A. Kaandorp [h], Giuseppe Falini [b,i], Zvy Dubinsky [j], Erik Caroselli [a,b,*], Stefano Goffredo [a,b]

[a] Marine Science Group, Department of Biological, Geological and Environmental Sciences, University of Bologna, Via F. Selmi 3, 40126 Bologna, Italy
[b] Fano Marine Center, The Inter-Institute Center for Research on Marine Biodiversity, Resources and Biotechnologies, Viale Adriatico 1/N, 61032, Fano, Italy
[c] Department of Marine and Coastal Sciences, Rutgers, The State University of New Jersey, New Brunswick, NJ, 08901, USA
[d] Institute for Marine Biological Resources and Biotechnology (IRBIM), National Research Council (CNR), Largo Fiera della Pesca 2, 60125, Ancona, Italy
[e] Department of Earth Sciences, University of Florence, via la Pira 4, Firenze, Italy
[f] Institute of Geosciences and Earth Resources (IGG), National Research Council of Italy (CNR), via la Pira 4, Firenze, Italy
[g] Institute of Materials Physics, Helmholtz-Zentrum Hereon, Max-Planck-Str. 1, 21502 Geesthacht, Germany
[h] Section Computational Science, Faculty of Science, University of Amsterdam, Science Park 904, room C3.147, 1090, GE, Amsterdam, the Netherlands
[i] Department of Chemistry "Giacomo Ciamician", University of Bologna, 40126, Bologna, Italy
[j] The Mina and Everard Goodman Faculty of Life Sciences, Bar-Ilan University, Ramat-Gan, 52900, Israel

## HIGHLIGHTS

- Characterization of an unexplored $CO_2$ vent cave
- $CO_2$ vents chemical-physical parameters affect ecological traits of calcifiers
- Aphotoendosymbiotic solitary coral naturally inhabiting a $CO_2$-rich gas environment.
- Prolonged acidified conditions did not affect *C. inornata* growth rate
- Shift towards an r-demographic strategy in response to acidified conditions

## GRAPHICAL ABSTRACT

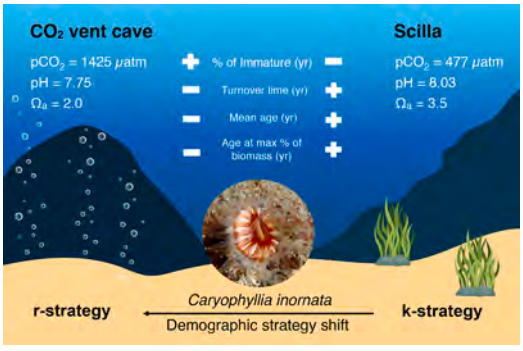


## ARTICLE INFO

*Keywords:*
Aphotoendosymbiotic coral
Mediterranean Sea
Population dynamics

## ABSTRACT

Submarine $CO_2$ volcanic vents represent peculiar environments with varying seawater chemical-physical parameters that may affect the ecological traits of calcifying organisms, such as growth and demographic characteristics. The present study focused on exploring the growth and population dynamics of a temperate, solitary and aphotoendosymbiotic coral *Caryophyllia inornata* (Duncan, 1878) living in a $CO_2$ vent cave at 14 m depth.

* Corresponding author at: Marine Science Group, Department of Biological, Geological and Environmental Sciences, University of Bologna, Via F. Selmi 3, 40126, Bologna, Italy.
*E-mail address:* erik.caroselli@unibo.it (E. Caroselli).
[1] These authors contributed equally to this work and share first authorship.

https://doi.org/10.1016/j.scitotenv.2025.180858
Received 9 March 2025; Received in revised form 29 October 2025; Accepted 30 October 2025
Available online 5 November 2025

Stress response
Demographic traits
Ocean acidification

The volcanic emissions in and around the cave led high levels of $pCO_2$, resulting in lower calcium carbonate saturation state ($\Omega_a$: 2.1–2.2) values compared to those observed in the ambient seawater of the Mediterranean Sea, not affected by venting activity. Prolonged acidified conditions ($pH_T$: 7.5) did not affect *C. inornata* growth rate but resulted in a population with higher percentage of juvenile individuals, lower average ages and a lower age at maximum biomass percentage, thus suggesting a transition in its population dynamics towards an r-demographic strategy. This study provides a detailed characterization of a previously unexplored $CO_2$ vent cave, highlighting the importance of these sites as natural laboratories to offer valuable insights into understanding the full ecological impact of aphotoendosymbiotic corals under ocean acidification.

## 1. Introduction

The rapid increase in greenhouse gas concentration due to anthropogenic activities is one of the main driving forces of global environmental climate change (Hassoun et al., 2022). Current $CO_2$ atmospheric levels (425.94 ppm, UCSanDiego, Scripps Institution of Oceanography, 2024) are determining shifts in ocean chemistry through an increase in dissolved $CO_2$ (Feely et al., 2023). High percentages of dissolved $CO_2$ lead to declines in seawater pH, carbonate ion concentration [$CO_3^{2-}$] and saturation state of aragonite/calcite ($\Omega_{a/c}$), in a process known as ocean acidification (OA; Feely et al., 2023). These changes in ocean chemistry are occurring at global and regional levels (Hassoun et al., 2022). According to IPCC's business-as-usual scenario (SSP5–8.5: high-emissions, low-mitigation scenario; IPCC, 2023), by 2100 average global [$CO_3^{2-}$] is projected to decrease by 48 %, which will lead to a decline in $\Omega_a$ from current values of ~3.2 to ~1.6 and $pH_T$ from ~8.05 to ~7.7 (Jiang et al., 2023).

The reduced availability of $CO_3^{2-}$ and $\Omega_{a/c}$ due to increasingly high $pCO_2$ in seawater negatively affects the precipitation of $CaCO_3$, hindering calcification processes and other key-life functions in different marine organisms that generate and accumulate calcium carbonate to produce skeletal hard parts, including molluscs, echinoderms, and corals (Fabricius et al., 2011). Although research has highlighted possible resilience among some coral species to OA (Teixidó et al., 2020), the impacts of prolonged exposure to acidified environments and conditions are still ambiguous and not fully understood (Vuleta et al., 2024). The outcomes of ocean acidification (OA) on coral physiological processes and other calcifying organisms have been largely investigated under controlled conditions in aquaria (Hahn et al., 2012). Although ex situ experiments may offer valuable insights into physiological responses to increasing acidification, they do not incorporate a wide array of factors (such as nutrient levels, irradiance, oxygenation, and species interactions), which characterize natural ecosystems and to which organisms are exposed in the wild (Hahn et al., 2012). More complete insights into species tolerance to OA may be gained by analyzing traits developed under local natural conditions (Teixidó et al., 2020). In this context, $CO_2$ vents represent unique environments that can serve as natural laboratories to investigate the potential long-term physiological and ecological impacts of OA (Foo and Byrne, 2021). Studies assessing the ecosystem-level effects of OA on marine organisms have been carried out at natural $CO_2$ seeps in Japan (Agostini et al., 2021) the Mariana Islands (Enochs et al., 2015), and Papua New Guinea (Fabricius et al., 2011). In the Mediterranean Sea, vent systems have been extensively studied at Panarea Island (Goffredo et al., 2014) and Ischia Island (Teixidó et al., 2020). Traits shaped by different evolutionary and ecological processes in response to natural OA conditions have been largely investigated in coral communities, including both those that naturally occur in these environments (Goffredo et al., 2014; Teixidó et al., 2020) and those experimentally transplanted to such sites (Agostini et al., 2021). Ocean acidification (OA), especially in combination with ocean warming, can negatively affect the growth and physiology of both temperate as well as tropical species, leading to a reduction in coral-dominated environments and severe habitat loss (Agostini et al., 2021).

Compared to photoendosymbiotic scleractinian corals (previously referred to as zooxanthellate corals), species without Symbiodiniaceae photoendosymbiosis (i.e. aphotoendosymbiotic corals, previously referred to as non - zooxanthellate corals) are significantly underrepresented in the literature (Vuleta et al., 2024).

Corals living without the reliance on photosynthesis products are heterotrophic and dependent on organic matter and plankton from the water column to support growth and other life processes (Vuleta et al., 2024). Nevertheless, the absence of light constraints enables these species to colonize broad geographical and bathymetric ranges and widely spread, representing approximately 50 % of known Scleractinian corals (Vuleta et al., 2024). In the context of the Anthropocene, aphotoendosymbiotic and solitary corals, such as *Caryophyllia inornata*, may have a higher chance of persisting as many symbiotic reef-building corals decline (Dishon et al., 2020). However, despite their potential resistance to ocean warming and acidification, their responses to global environmental changes remain understudied, highlighting the need to address this knowledge gap.

The present study focused on the temperate-subtropical scleractinian aphotoendosymbiotic coral *Caryophyllia inornata* (Fig. 1A; Duncan 1878), a solitary species widely distributed in the Mediterranean Sea and Northeastern Atlantic Ocean, from the Canary Islands to the United Kingdom (Zibrowius, 1980). The lack of photoendosymbiotic dinoflagellate allows *C. inornata* to colonize shaded and dimly lit hard substrates, such as vertical walls, crevices, and vaults of caves or wrecks up to 100 m depth (Zibrowius, 1980). It is a gonochoric and brooding coral with an unusual and continuous production of agamic embryos in male, female, and sexually inactive polyps (Marchini et al., 2015). *Caryophyllia inornata* growth, demography and reproductive responses to temperature have been widely investigated along a latitudinal gradient on the Western Italian Coast (Caroselli et al., 2015, 2016; Marchini et al., 2020). Nevertheless, the effects of acidified conditions on *C. inornata* are still unknown. This study aimed to examine the effects of long-term exposure to acidified conditions on the growth and population dynamics of this solitary, aphotoendosymbiotic scleractinian species, naturally inhabiting a newly discovered cave within the hydrothermal system of Panarea Island (Italy; Fig. 1) and to characterize the environmental conditions of this previously uncharted site.

## 2. Materials and methods

### 2.1. Study site

The study was performed close to Panarea Island in the Aeolian Archipelago (Southeastern Tyrrhenian Sea, Italy, 38° 38′ 14″ N, 15° 4′ 2″ E; Fig. 2). This area is part of an active volcanic system characterized by hydrothermal water and gas exhalations that are temporally and spatially variable in their geochemical composition (Goffredo et al., 2014). Several emission spots have been identified from the seafloor at shallow depths by direct observations and bathymetric investigations (Capaccioni et al., 2005). The study was conducted at a submerged cave located at a depth of 14 m off Basiluzzo Island (Fig. 2; Fig. 3a-b). The site is characterized by hydrothermal emissions sweeping from the seabed in proximity and within the cave.

Three experimental sites were selected to investigate potential environmental gradients from the exterior to the interior of the $CO_2$ vent

cave, enabling a detailed examination of how $CO_2$ venting from the seabed influences the surrounding conditions.

One site was located on the external vault at the cave entrance, while the other two were positioned on opposite walls inside (Fig. 3a). The site of Scilla (38° 16′ 15″ N, 15° 42′ 30″ E; Fig. 2), located along the western coast of Italy, was chosen as a comparative site for environmental and biological parameters. This site was selected as a reference because of its latitudinal proximity to the study area, the absence of volcanic influence, and the documented presence of the coral *C. inornata* inhabiting shaded crevices at depths comparable to those of the acidified cave (Fig. 2; Caroselli et al., 2016). In addition, the growth and demographic traits of the local *C. inornata* population have already been characterized in a previous study following analogue methods (Caroselli et al., 2016).

### 2.2. Environmental parameters and carbonate chemistry

Environmental parameters were recorded at each of the three sites within the $CO_2$ vent cave during six surveys conducted in the warm months between July 2019 and July 2023. Environmental parameters were collected during each survey, lasting 3–5 days, with data obtained from one dive per day, resulting in approximately 12–15 measurements per site per day. Depth (m), temperature (°C), salinity (PSU), and $pH_{NBS}$ (National Bureau of Standards scale) were recorded using a multiparameter probe (600R, YSI Incorporated). Seawater samples for total alkalinity ($A_t$, μmol/kg) were collected at each site and stored at 4 °C in amber 100 mL glass bottles upon poisoning with 1 % of saturated mercuric chloride ($HgCl_2$) to avoid biological alterations (Goffredo et al., 2014). $A_t$ measurement were performed by Gran titration using a 702 SM Titrino (Metrohm AG, Italy). The reliability of titration measurements was previously cross-validated using certified reference materials for oceanic $CO_2$ measurements, yielding $A_t$ values comparable to those provided in the product certificate of analysis (2203.56 ± 0.75 $\mu mol \cdot kg^{-1}$; Batch 187 and Batch 213 from the Andrew Dickson Laboratory, Scripps Institution of Oceanography, UC San Diego). The carbonate chemistry of seawater at the study site was calculated using CO2SYS software (Lewis et al., 1998), based on depth, temperature, salinity, $pH_{NBS}$ and $A_t$ values, while considering referenced dissociation constants (Uppström, 1974; Dickson and Millero, 1987). To quantify dissolved inorganic nutrients (ammonium–$NH_4$, nitrite–$NO_2$, nitrate–$NO_3$, orthophosphate–$PO_4$, and orthosilicate–$SiO_4$), seawater samples were filtered (GF/F Whatman) and immediately stored at −22 °C in polyethylene vials until analysis. Nutrients were analyzed using colorimetric methods (Parsons et al., 1984), and the analyses were carried out at the Institute for Marine Biological Resources and Biotechnology. Mean daily values of physical environmental parameters (depth, temperature, salinity, $pH_T$, and $A_t$) and dissolved inorganic nutrients of Scilla were obtained from the Copernicus Marine Data Store (Feudale et al., 2023). To ensure temporal consistency in comparisons, only data from Scilla corresponding to the months of the environmental surveys conducted in the $CO_2$ vent cave were considered. Using these data, the carbonate chemistry of seawater at Scilla was calculated employing the CO2SYS software while considering referenced dissociation constants (Lewis et al., 1998; Uppström, 1974; Dickson and

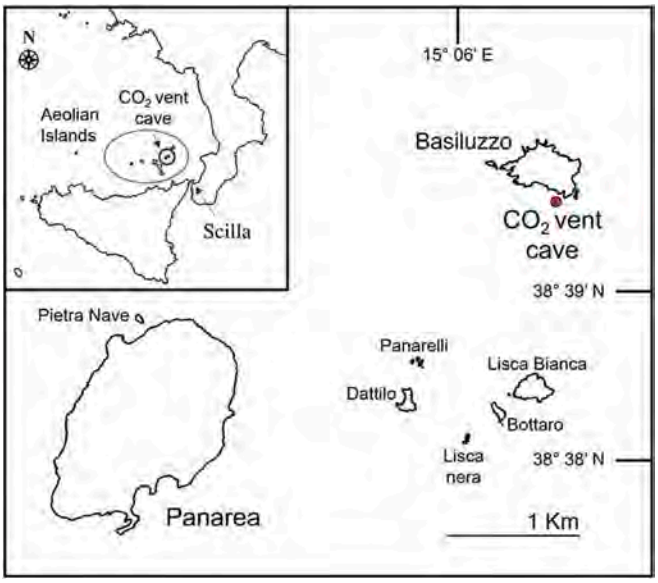


**Fig. 2.** Map of Southern Italy (top left corner) highlighting the Aeolian archipelago and the site of Scilla. The $CO_2$ vent cave, located near the Panarea Island and close to Basiluzzo, is marked with a red dot.

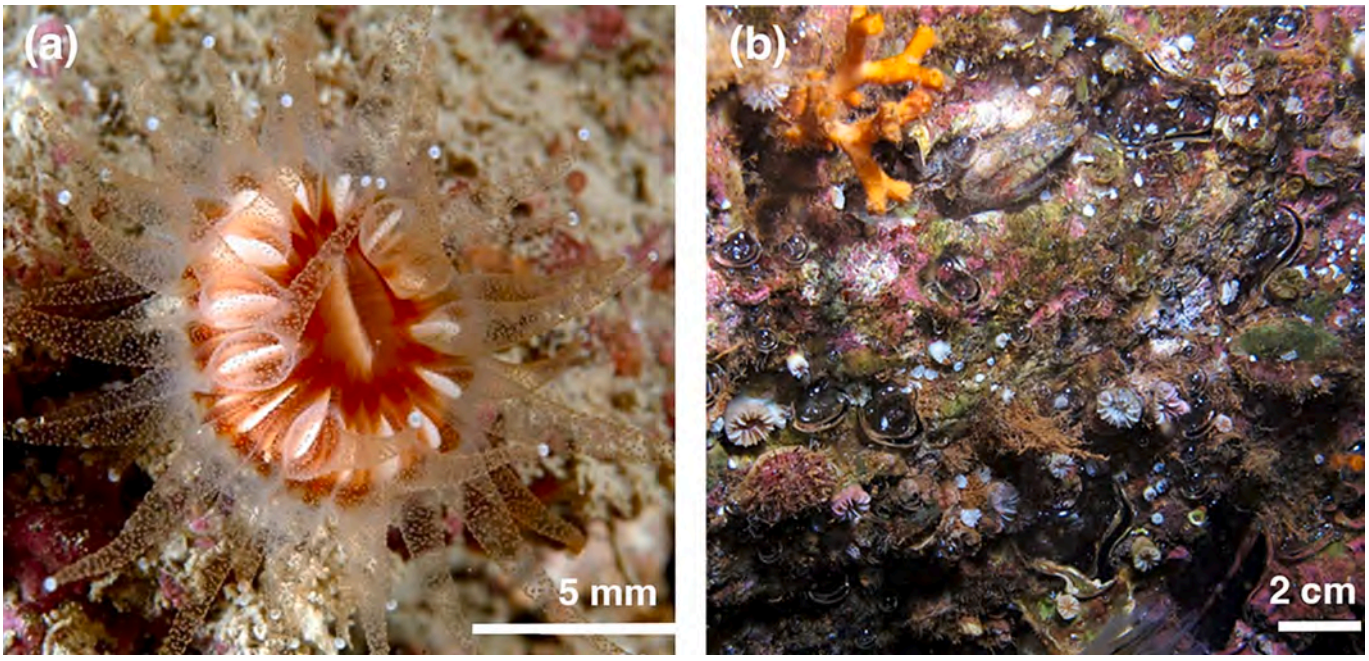


**Fig. 1.** (a) Living specimen of *Caryophyllia inornata*. (b) *Caryophyllia inornata* surrounded by $CO_2$ bubbles trapped on the rock wall of the cave.

Millero, 1987) as for the $CO_2$ vents cave.

### 2.3. Geochemical characterization of bubbling gas emissions

Gas emissions from the seabed around the cave were sampled in July 2020, May 2021 and July 2023, using 50-ml thorion-tapped glass tubes that had been pre-weighted, evacuated, and filled with 20 mL of a 0.15 M $Cd(OH)_2$ and 4 M NaOH suspension. Gas emissions were analyzed with gas-chromatographs (Shimadzu 14a-15a, see detail in Supplementary Information; Capaccioni et al., 2005). Seawater was also sampled to 12 cc plastic tubes filled with 2 mL of $Cd(NH_4)_2$ solution to analyse the reduced S species (including dissolved $H_2S$, $HS^-$ and $S^{2-}$) as $SO_4^{2-}$ after oxidation with $H_2O_2$ by ionic chromatography (Montegrossi et al., 2006). Gas and dissociated ions analyses were performed at the Laboratory of Fluid Geochemistry of the University of Florence.

### 2.4. Coral sample collection and analysis

Coral sampling took place in July 2020. At each site, *Caryophyllia inornata* specimens were haphazardly collected with a hammer and a chisel (Site 1, $n = 44$; Site 2, $n = 48$; Site 3, $n = 39$) and photoquadrats were taken using square patches of 10 cm*10 cm (0.01 $m^2$ each; Site 1, $n = 16$; Site 2, $n = 16$; Site 3, $n = 6$). Collected specimens were immersed in a 10 % solution of commercial bleach to remove coral tissue and dried at a low temperature (50 °C) to avoid phase transitions in the skeletal mineral composition (Vongsavat et al., 2006). Coral skeletons were then observed under a stereoscope to remove fragments of substratum or calcareous deposits from epibionts. The biometric measurements (L: maximum axis of the oral disc; W: polyp weight; h: polyp height), and the skeletal dry mass (M) of collected samples were measured with a caliper and a precision balance, respectively (Caroselli et al., 2016). Within each photoquadrat the sampling area ($m^2$), perimeter (cm), area ($cm^2$) and length (mm) of each observed individual and the total amount of individuals ($N_{ph}$) were measured using the software ImageJ (Schindelin et al., 2012). The dry skeletal mass (M) of individuals observed in the photoquadrats was estimated using the M/L relationship from collected samples. The number of individuals ($N_{ph}$), dry skeletal masses (M) and sampling areas ($m^2$) of each photoquadrat were used to estimate population density parameters: population abundance (N $m^{-2}$) and mass per square meter (g $m^{-2}$). The percent cover (% Area) was obtained from the full coverage of *C. inornata* ($cm^2$) and the total substrate area ($cm^2$; Caroselli et al., 2015).

### 2.5. Coral age determination

A subset of 32 specimens ($n_{CT}$,; Site 1, $n = 9$; Site 2, $n = 8$; Site 3, $n = 6$) was randomly selected from collected corals and analyzed through synchrotron radiation based X-Ray μCT at the imaging beamline P05 (Wilde et al., 2016) operated by Helmholtz-Zentrum Hereon at the storage ring PETRA III at Deutsches Elektronen-Synchrotron (DESY;

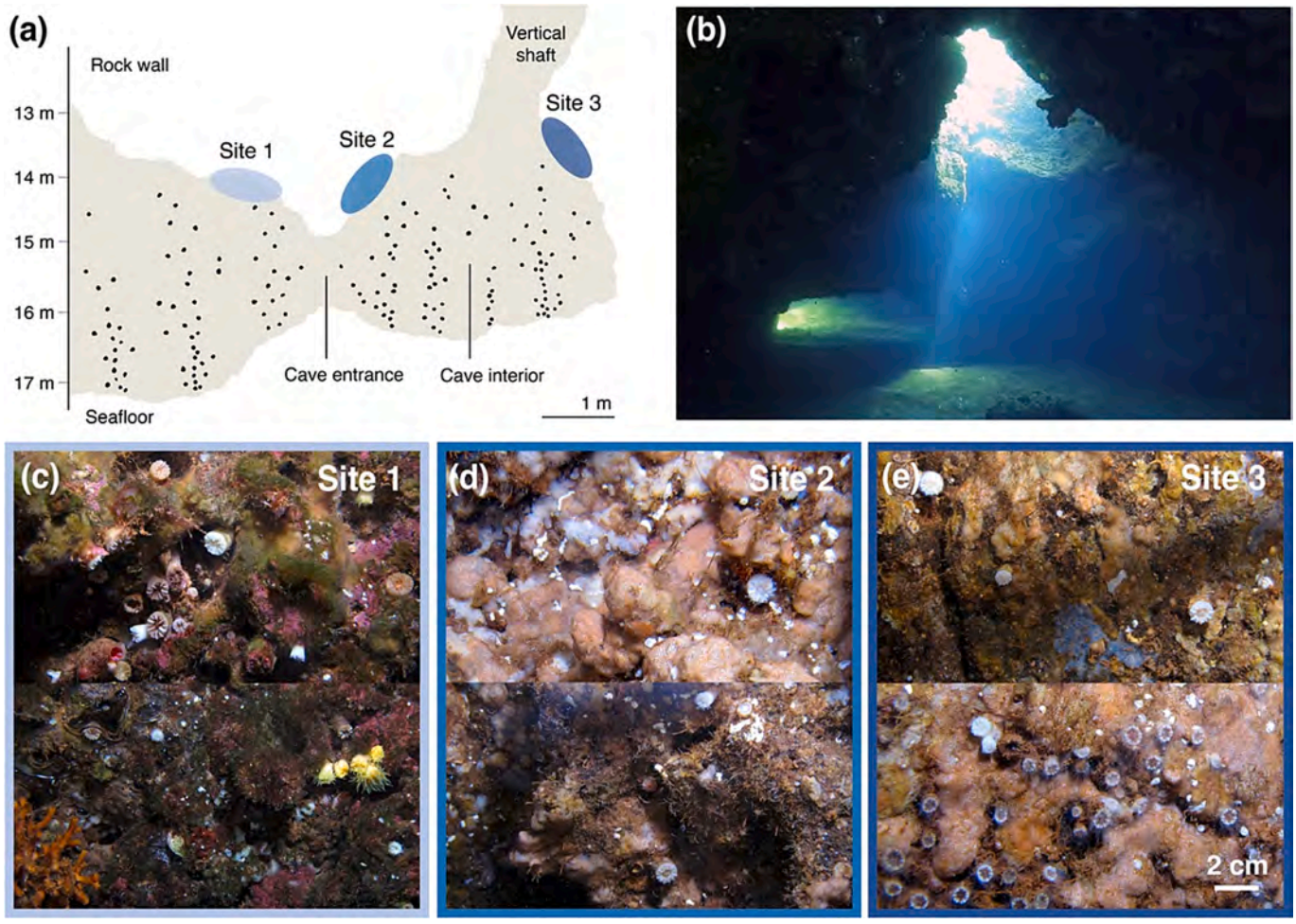


**Fig. 3.** (a) Profile of the submerged $CO_2$ vent cave with gas emissions from the seabed (black dots). Experimental sites and respective depths are: Site 1 (light blue): 14.2 m; Site 2 (blue): 14.2 m; Site 3 (dark blue): 13.5 m. (b) Photograph taken from the cave entrance, showing the interior with light streaming in through the vertical shaft. (c-d-e) Seascape of site 1, 2, and 3, respectively, showing associated species, such as the coral *Leptopsammia pruvoti* and the bryozoan *Myriapora truncata* at Site 1, bryozoans of the genus *Schizoporella* at Site 2 and 3, and the coral *Polycyathus muellerae* at Site 3.

Germany). The resulting scans were elaborated to establish coral age (yr) through sclerocronology by counting high-density bands (Caroselli et al., 2016) using the software ImageJ (Schindelin et al., 2012).

### 2.6. Growth modelling

The mean annual growth rate was estimated by dividing polyp length (*L:* maximum axis of the oral disk; Caroselli et al., 2019) by its age (yr). The relationships between mean annual growth and individual age displayed a negative exponential relationship, allowing the application of the von Bertalanffy growth model (Von Bertalanffy, 1938):

$$L_t = L_\infty \left(1 - e^{-kt}\right) \quad (1)$$

where $L_t$ = individual length at age $t$; $L_\infty$ = asymptotic length; $k$ = growth constant; $t$ = individual age. The mean value and confidence interval (CI) of $L_\infty$ and $k$ were estimated for each site through a regression analysis by least squares procedure developed with the software MATLAB R2022b (The MathWorks Inc., 2022; Caroselli et al., 2016). The resulting von Bertalanffy age-length function was applied to assess the age (yr) of individuals from the photoquadrats based on their $L$, thus obtaining population age-frequency distributions.

### 2.7. Demography

Since younger age classes are difficult to observe and collect in the field, the application of the Beverton and Holt demographic model (Beverton and Holt, 1956) allowed the reconstruction of the youngest classes and theoretical population age structure at each site (Caroselli et al., 2016). Observed population age-frequency distribution analysis was used to establish the theoretical model through the linear regression of the natural logarithm of the number of individuals in each age class ($N_t$, frequency) against the corresponding age ($t$) expressed as:

$$\ln N_t = at + b. \quad (2)$$

The slope $a$ changed in sign defines the instantaneous rate of mortality (Z), corresponding to the decrement of the number of corals with age, while the intercept $b$ indicates the natural logarithm of the number of individuals at age zero ($N_0$) (Pauly, 1984; Caroselli et al., 2016). To estimate the mortality rate, this method assumes the condition of a steady-state population, that requires no missing or overrepresented age cohort due to disturbance events that might have altered recruitment patterns (Grigg, 1984). In a theoretical steady-state population, the variance in the frequency of age classes should be explained by age (i.e., $r^2$ of the regression line equal to one). Regression lines with lower $r^2$ would display populations deviating from the steady state (Sparre and Venema, 1989; Caroselli et al., 2016). The turnover time was obtained as $Z^{-1}$ (Pauly, 1984; Goffredo et al., 2010). The instantaneous rate of mortality ($Z$) was then used to express the survivorship curve as the numeric reduction of individuals over time:

$$N_t = N_0 e^{-Zt} \quad (3)$$

Considering the survival curve, the age at which <0.5 % of the population was still surviving was defined as the maximum individual lifespan (Sparre and Venema, 1989). The cohort yield was obtained by multiplying dry skeletal mass at each age class by the respective percentage of survival. The observed percentage of immature individuals was determined by the sum of frequencies of the age classes below sexual maturity (corresponding to 8 yr, Marchini et al., 2015). The theoretical percentage of immature individuals was obtained by summing the frequencies of the theoretical number of individuals in the age classes below sexual maturity. The observed mean age was calculated as the mean ages of collected samples dated using the growth curve. The theoretical mean age was obtained from the theoretical number of individuals for each age class. The observed biomass-age distribution was estimated by summing individual mass in each age class while the theoretical distribution was determined by multiplying the theoretical number of individuals in each age class for the expected biomass at that age. The observed mean age of biomass was obtained by summing the products of the observed biomass in each age class multiplied by its age and then dividing the sum by the total observed biomass. The theoretical mean age of biomass was estimated using the same method but with the theoretical biomass. Observed and theoretical ages at the maximum percentage of biomass were defined as the age class corresponding to the highest percentage of biomass in the respective distributions. The age at maximum biomass provided the threshold after which mortality will prevail on biomass increment due to growth and population biomass will decrease (Beverton and Holt, 1956; Caroselli et al., 2016).

### 2.8. Statistical analysis

The average of each environmental parameter was calculated by combining data from all surveys.

Physical environmental and carbonate chemistry parameters did not follow normal distributions, so Kruskal-Wallis test was applied as a nonparametric alternative to ANOVA to test for differences in these parameters among the sites (Potvin and Roff, 1993). After a significant Kruskal-Wallis test result, post-hoc pairwise multiple comparisons were conducted with the Dunn test with 5 % statistical significance ($p$-value adjustment method: Benjamini-Hochberg) (Dunn, 1964; Benjamini and Hochberg, 1995). One-way analysis of variance (ANOVA) was used for the dissociated ion concentrations, as they met the assumptions, and Tukey's Honestly Significant Difference (HSD) was performed as a post-hoc test.

Pearson correlation coefficient was used to test the correlation between $L$ and age in the mean annual growth rate. Nonparametric Kolmogorov-Smirnov test was performed to test for differences in the age frequency distribution among sites. Statistical analyses were computed using IBM SPSS Statistics 28.0 (IBM Corp, 2021) and RStudio software (Posit team, 2023; R Core Team, 2024).

## 3. Results

### 3.1. Environmental analysis and carbonate chemistry

Temperature, salinity, total alkalinity, and all the dissolved inorganic nutrients were homogeneous across the three sites (Table 1, S1; Fig. 4). Temperature, salinity and total alkalinity at the $CO_2$ vent cave showed lower values compared to those at Scilla (Dunn's test $p < 0.05$, Table 1; Fig. 4). Specifically, the three sites at the $CO_2$ vent cave were approximately 1.5 °C colder and had lower salinity compared to Scilla (35.8 PSU vs. 37.8 PSU, respectively; Table 1; Fig. 4). Phosphate levels also differed between the cave and the control site, with higher contents of this nutrient found at the $CO_2$ vent cave (Dunn's test $p < 0.05$, Table S1). For carbonate chemistry parameters, $pH_T$, $pCO_2$, $CO_3^{2-}$, $CO_2$, $\Omega_c$, $\Omega_a$ were homogeneous across the three cave sites (Table 1) but differed significantly from those at the control site in Scilla (Table 1). Notably, the $CO_2$ vent cave sites exhibited significantly higher $pCO_2$ levels (ranging from approximately +153 % to +262 %) and reductions in $pH_T$ (−3.5 %), carbonate ions concentration ($CO_3^{2-}$, −44 %) and calcium carbonate saturation state ($\Omega_a$ and $\Omega_c$, both reduced by −43 %; Table 1) compared to the seawater conditions at Scilla.

### 3.2. Bubbling gas emissions

The gaseous emissions were predominantly composed of $CO_2$ (98.7 %), with smaller proportions of $N_2$ (0.78 %), $H_2S$ (0.42 %), $O_2$ (0.07 %), $H_2$ (0.02 %), Ar (0.02 %), and $CH_4$ (0.01 %) by volume (Table 2). Other minor gas compounds (Ne, CO, $H_2$, He and light hydrocarbons) resulted in percentages below 0.01 %. Dissociated ion concentrations did not differ among the three sites at the $CO_2$ vent cave, except for $HS^-$, which was higher in Site 3 (mean value: 10.93 mg L-1) compared to Site 1 and

**Table 1**
Physical environmental parameters and carbonate chemistry parameters at the three sites within the $CO_2$ vent cave and at the control site of Scilla. $A_t$, total alkalinity, DIC, dissolved inorganic carbon, $\Omega_c$ and $\Omega_a$, calcite and aragonite saturation state. Data are presented as mean ± 95 % CIs, $n$ = number of samples. Different letters indicate statistical differences by Kruskal-Wallis followed by post-hoc Dunn's test ($p \leq 0.05$).

| | $CO_2$ vents cave | | | Control Site |
|---|---|---|---|---|
| | Site 1 | Site 2 | Site 3 | Scilla |
| | $n = 137$ | $n = 123$ | $n = 166$ | $n = 185$ |
| **Temperature (°C)** | 20.86 ± 0.31[a] | 20.98 ± 0.34[a] | 20.50 ± 0.31[a] | 22.13 ± 0.41[b] |
| **Salinity (PSU)** | 35.78 ± 0.06[a] | 35.84 ± 0.05[a] | 35.83 ± 0.04[a] | 37.84 ± 0.03[b] |
| | $n = 15$ | $n = 14$ | $n = 14$ | $n = 185$ |
| **$A_t$ (µmol/kg)** | 2380 ± 70[a] | 2357 ± 129[a] | 2368 ± 88[a] | 2640 ± 3[b] |
| | $n = 137$ | $n = 123$ | $n = 166$ | $n = 185$ |
| **$pH_T$** | 7.74 ± 0.06[a] | 7.78 ± 0.06[a] | 7.73 ± 0.06[a] | 8.03 ± 0.00[b] |
| **$pCO_2$ (µatm)** | 1341 ± 247[a] | 1208 ± 249[a] | 1725 ± 614[a] | 477 ± 6[b] |
| **$HCO_3^-$ (µmol/kg)** | 2042 ± 40[a] | 1961 ± 48[b] | 2042 ± 41[a] | 2083 ± 1[c] |
| **$CO_3^{2-}$ (µmol/kg)** | 128 ± 11[a] | 135 ± 12[a] | 128 ± 11[a] | 230 ± 1[b] |
| **$CO_2$ (µmol/kg)** | 42.84 ± 8.05[a] | 38.35 ± 8.06[a] | 55.10 ± 19.38[a] | 14.30 ± 0.06[b] |
| **DIC (µmol/kg)** | 2213 ± 37[a] | 2134 ± 45[b] | 2224 ± 44[a] | 2327 ± 2[c] |
| **$\Omega_c$** | 3.05 ± 0.26[a] | 3.20 ± 0.28[a] | 3.03 ± 0.25[a] | 5.38 ± 0.03[b] |
| **$\Omega_a$** | 1.99 ± 0.17[a] | 2.09 ± 0.19[a] | 1.98 ± 0.16[a] | 3.53 ± 0.02[b] |

Site 2 (respectively 2.77 and 4.00; Tukey's test $p < 0.05$, Table S2).

### 3.3. Coral growth

At each of the three site within the $CO_2$ vent cave, specimens dated using CT scans showed an exponential decrease in mean growth rate with increasing coral age (Fig. 5), consistent with the typical growth pattern of solitary corals, including *C. inornata* in other locations along the Italian Tyrrhenian coasts (Caroselli et al., 2016). The age variance of dated samples explained 56–76 % of the mean growth rate variation (Site 1: $R^2 = 0.555$; Site 2: $R^2 = 0.642$; Site 3: $R^2 = 0.761$; Fig. 5A). For each site, population growth parameters ($L_\infty$: asymptotic length; *k:* growth constant) and their respective 95 % confidence intervals were calculated (Table 3). Since $L_\infty$ and $k$ were homogenous among sites (95 % CIs overlapped; Table 5), the von Bertalanffy growth functions yielded similar predicted sizes at each age (Fig. 5B). Therefore, data from individuals dated through sclerochronology across all populations were pooled to estimate the general growth parameters: $L_\infty$= 19.2 mm (95 % CI = 11.2–27.2; Table 3) and $k$ = 0.066 (95 % CI = 0.028–0.103; Table 3). The resulting von Bertalanffy growth curve describing the general age-length relationship across all sites (Fig. 5B) allowed the determination of age (yr) for all corals identified in the photoquadrats (Table 3). The general growth parameters obtained from the population at the $CO_2$ vent cave and their 95 % CI ranges were then compared with those from the Scilla population (Caroselli et al., 2016), showing no significant differences (95 % CI overlapped; Table 3).

### 3.4. Population age structure

Population abundance (N $m^{-2}$) showed no significant differences among sites (Table 4), while lower mean values of mass per square meter (g $m^{-2}$) and percent cover (% Area) were observed in the cave sites compared to Scilla (Table 4). The age-frequency distributions (Fig. 6) differed among the three sites at the $CO_2$ vent cave (Kolmogorov-Smirnov test, $p < 0.05$), therefore observed and theoretical population

**Table 2**
Gas emission composition from the seabed around the cave. Data are presented as mean ± 95 % CIs, $n$ = number of samples.

| | $CO_2$ vent cave |
|---|---|
| | $n = 10$ |
| **$CO_2$ (%)** | 98.7 ± 0.3 |
| **$N_2$ (%)** | 0.78 ± 0.12 |
| **$H_2S$ (%)** | 0.42 ± 0.39 |
| **$O_2$ (%)** | 0.07 ± 0.01 |
| **$H_2$ (%)** | 0.02 ± 0.01 |
| **Ar (%)** | 0.02 ± 0.00 |
| **$CH_4$ (%)** | 0.01 ± 0.00 |

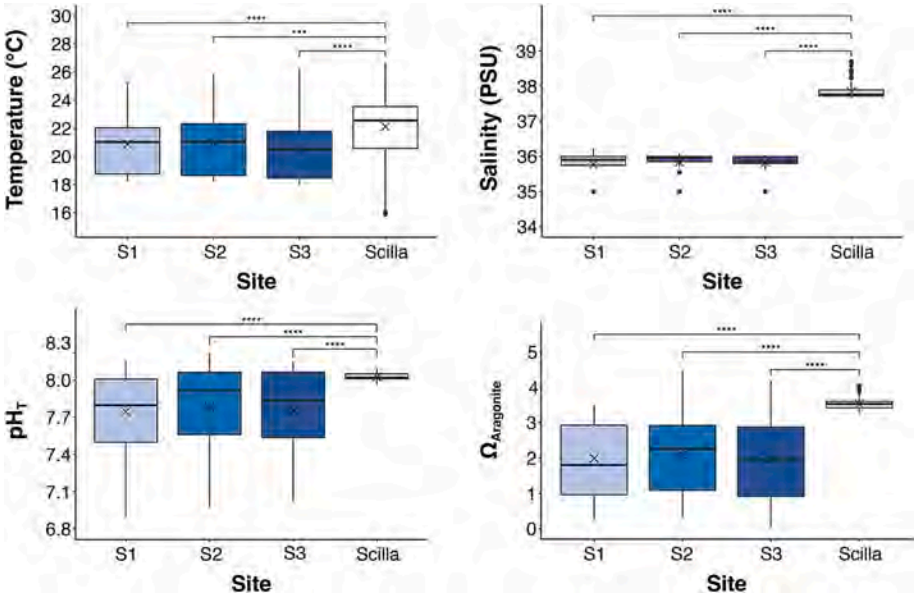


**Fig. 4.** Boxplots showing data variability within sites. Temperature, salinity, $pH_T$ and $\Omega_a$ at the three sites within the $CO_2$ vent cave (Site 1, light blue; Site 2, blue; Site 3, dark blue) and at the control site of Scilla (white boxes). The crosses indicate the mean values. Temperature, $n = 641$; salinity, $pH_T$, and $\Omega_a$ $n = 611$. Significant differences are denoted by *** (Dunn's test, $p < 0.05$).

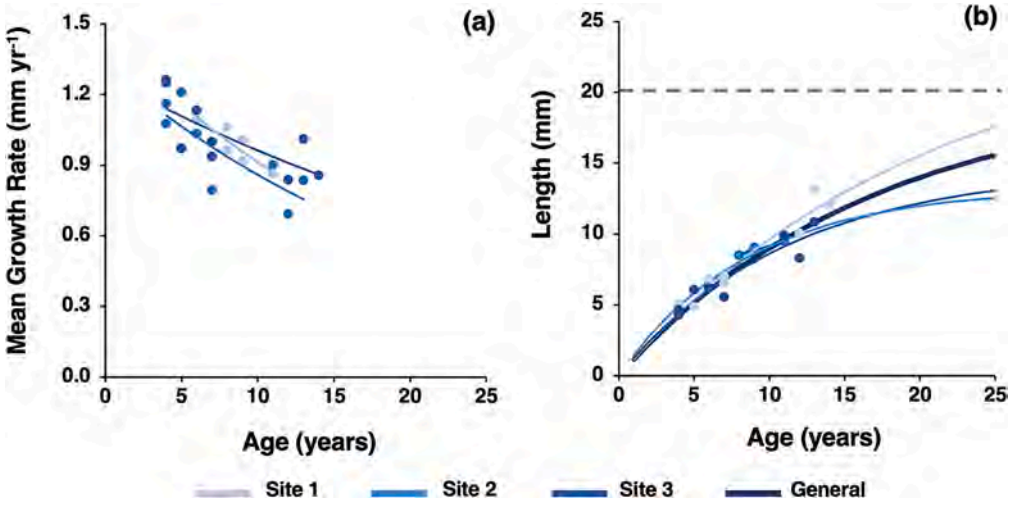


**Fig. 5.** Mean growth rate and age-length von Bertalanffy growth curve at the three sites within the $CO_2$ vent cave. Points indicate samples dated by CT scans. (a) Relationships between mean growth rate and age. Site 1: $R^2 = 0.555$, $p < 0.05$; Site 2: $R^2 = 0.642$, $p < 0.05$; Site 3: $R^2 = 0.761$, $p < 0.05$. (b) Age-length von Bertalanffy. Dashed line indicates the maximum expected length of corals for all populations ($L_\infty = 19.2$ mm). Number of collected corals: Site 1, $n = 9$; Site 2, $n = 8$; Site 3, $n = 6$.

**Table 3**
Growth parameters at the three sites within the $CO_2$ vent cave and at the control site of Scilla. $n_{CT}$, number of collected corals dated by CT scans; $n_{Ph}$, number of individuals from photoquadrats dataset dated using general growth curve; $L_\infty$: asymptotic length; *k:* growth constant; mean age of collected samples at each site. Ranges in brackets indicate 95 % CI.

| | $CO_2$ vent cave | | | | Control Site |
|---|---|---|---|---|---|
| | Site 1 | Site 2 | Site 3 | General | Scilla* |
| $n_{CT}$ | 9 | 8 | 6 | 23 | 35 |
| $n_{Ph}$ | 95 | 83 | 24 | 180 | 47 |
| $L_\infty$ (mm) | 24.9 ± 21.0 | 14.7 ± 9.7 | 13.3 ± 7.5 | 19.2 ± 8.0 | 12.3 ± 5.3 |
| *k* | 0.049 ± 0.054 | 0.089 ± 0.092 | 0.116 ± 0.114 | 0.066 ± 0.037 | 0.101 ± 0.079 |

* Caroselli et al., 2016

**Table 4**
Observed and theoretical demographic parameters at the three sites within the $CO_2$ vent cave and at the control site of Scilla (Caroselli et al., 2016). $n_{Ph}$, number of individuals from photoquadrats. Data are presented as mean ± 95 % Cis. Different letters indicate statistical differences by Kruskal-Wallis followed by post-hoc Dunn's test ($p \leq 0.05$).

| | $CO_2$ vent cave | | | Control Site |
|---|---|---|---|---|
| | Site 1 | Site 2 | Site 3 | Scilla* |
| $n_{Ph}$ | 95 | 83 | 24 | 47 |
| **Population abundance (N $m^{-2}$)** | 594 ± 131 | 519 ± 246 | 400 ± 263 | 783 ± 217 |
| **Mass per square meter (g $m^{-2}$)** | 258 ± 92[a] | 67 ± 35[b] | 43 ± 52[b] | 287 ± 95[a] |
| **Percent cover (% Area)** | 1.85 ± 0.53[a] | 0.72 ± 0.40[b] | 0.52 ± 0.41[b] | 2.75 ± 0.83[a] |
| **Stability $R^2$** | 0.611 | 0.669 | 0.465 | 0.437 |
| **Instantaneuos rate of mortality Z ($yr^{-1}$)** | 0.148 | 0.343 | 0.199 | 0.102 |
| **Turnover time (yr)** | 7 | 3 | 5 | 10 |
| **Observed % of immature** | 55 | 94 | 92 | 43 |
| **Theoretical % of immature** | 70 | 94 | 80 | 51 |
| **Observed mean age (yr)** | 7.5 ± 0.8 | 4.2 ± 0.5 | 4.0 ± 0.9 | 8.3 ± 1.1 |
| **Theoretical mean age (yr)** | 6 | 2 | 4 | 9 |
| **Observed age at max % of biomass (yr)** | 8 | 7 | 9 | 10 |
| **Theoretical age at max % of biomass (yr)** | 13 | 6 | 11 | 15 |
| **Observed mean age of biomass (yr)** | 11 | 6 | 7 | 11 |
| **Theoretical mean age of biomass (yr)** | 16 | 8 | 14 | 21 |

* Caroselli et al., 2016

demographic parameters were estimated for each site (Table 4, Fig. 6). Since these parameters are estimated from the observed population structure at each site and from the corresponding demographic model (Beverton and Holt, 1956), they represent net values and have no associated uncertainty. Therefore, comparisons among sites were made directly using the estimated net values, as no statistical tests could be applied. The observed age-frequency distributions provided the instantaneous rate of mortality (Z: Site 1 = 0.148; Site 2 = 0.343; Site 3 = 0.199; Table 4) and population structure stability ($R^2$: Site 1 = 0.611; Site 2 = 0.669; Site 3 = 0.465; Table 4). Observed populations were

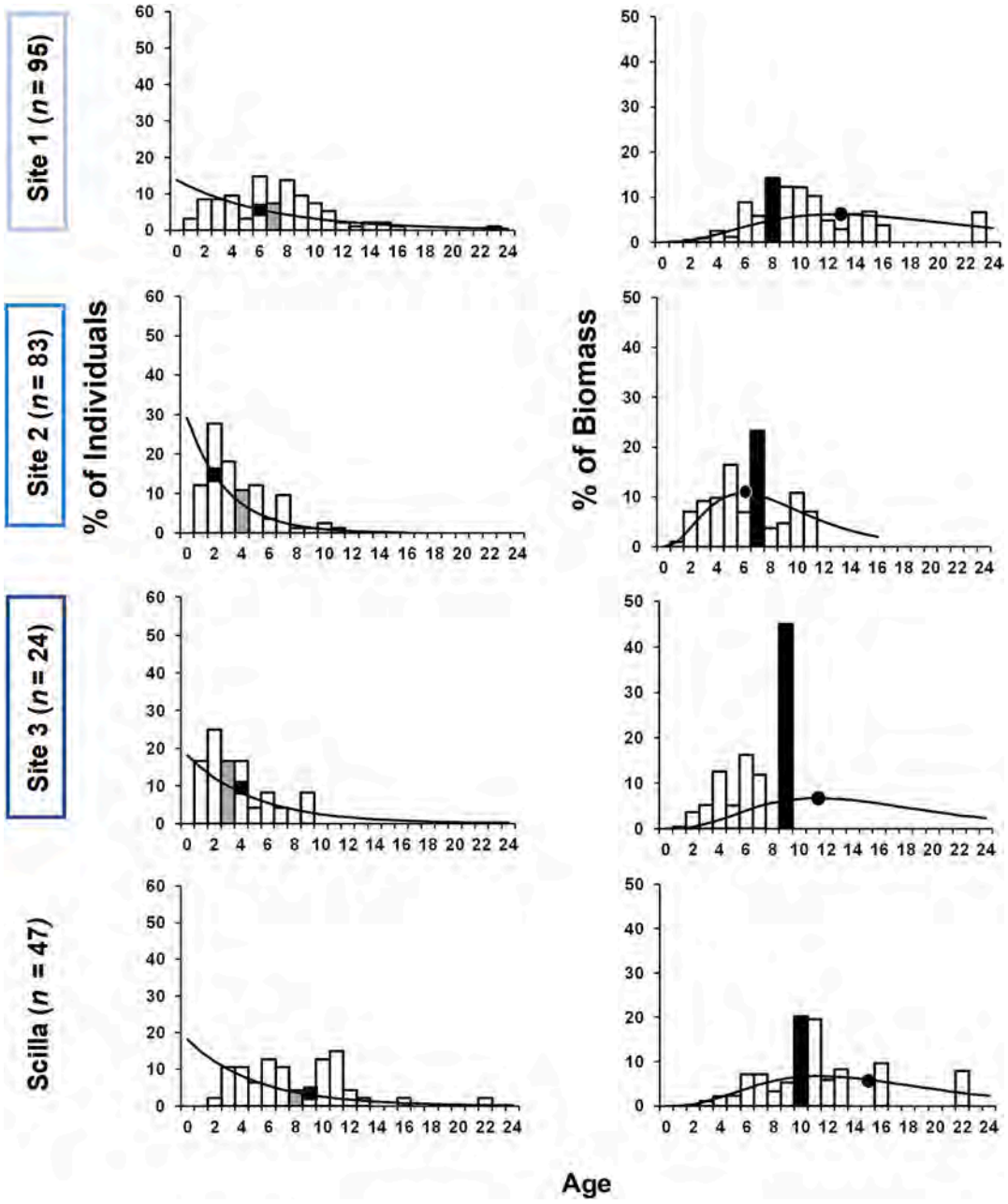


**Fig. 6.** Age class structure by abundance and percentage of biomass of populations of *C. inornata* at the three sites within the $CO_2$ vent cave. The observed age class containing the mean age of the sampled individuals (grey column) and the observed age at maximum percentage of biomass (black column) are indicated. The lines represent the theoretical distributions of percentage of individuals and percentage of biomass. The theoretical age class containing the mean age of individuals (black square) and the theoretical age at maximum percentage of biomass (black dot) are represented. Asterisks correspond to the age at sexual maturity (8 yr corresponding to ~6.1 mm in length, Marchini et al., 2015; Caroselli et al., 2016).

mainly dominated by young individuals below the size of sexual maturity (~6.1 mm in length, corresponding to 8 yr; Marchini et al., 2015; Caroselli et al., 2016; Fig. 6). Populations included a high percentage of juvenile individuals (Observed % of immature: Site 1 = 55; Site 2 = 94; Site 3 = 92, Table 4), determining an observed mean age lower than the sexual maturity threshold (Observed mean age: Site 1 = 7.5; Site 2 = 4.2; Site 3 = 4.0; Table 4; Fig. 6). Also considering parameters from the theoretical distributions, populations were dominated by juvenile individuals (Theoretical % of immature: Site 1 = 70; Site 2 = 94; Site 3 = 80; Table 4) which determined a theoretical mean age below the sexual maturity in each site (Theoretical mean age: Site 1 = 6; Site 2 = 2; Site 3 = 4; Table 4; Fig. 6). Site 1 had older individuals and a lower percentage of immature polyps compared to the other two sites and was the only population where the observed mean age of biomass exceeded the sexual maturity threshold (Observed mean age of biomass: Site 1 = 11; Site 2 = 6; Site 3 = 7; Table 4). The theoretical model suggested a biomass distribution shifted towards sexually mature age classes in all sites (Theoretical mean age of biomass: Site 1 = 16; Site 2 = 8; Site 3 = 14; Table 4). Site 2 resulted in age at maximum percentage of biomass (both observed and theoretical) below the sexual maturity threshold (Observed age at max % of biomass: Site 1 = 8; Site 2 = 7; Site 3 = 9; Theoretical age at max % of biomass: Site 1 = 13; Site 2 = 6; Site 3 = 11; Table 4; Fig. 6). Compared to Scilla (Caroselli et al., 2016; Table 4), the population at the $CO_2$ vent cave exhibited a shorter turnover time (3–7 yr compared to 10 yr at Scilla), a higher percentage of immature individuals (observed % of immature individuals ranging from 55 to 94 % compared to 43 % at

Scilla and theoretical % of immature individuals ranging from 70 to 94 % compared to 51 % at Scilla), lower mean age values (observed mean age ranging from 4.0 to 7.5 yr compared to 8.3 yr at Scilla and theoretical mean age ranging from 2 to 6 yr compared to 9 yr at Scilla. Table 4) and lower age at maximum biomass percentage (observed age ranging from 7 to 9 yr compare to 10 yr at Scilla and theoretical age ranging from 6 to 13 yr compared to 15 yr at Scilla; Table 4).

## 4. Discussion

This study represents the first investigation of this hydrothermal system, a previously unexplored site in the Mediterranean Sea, as a natural laboratory with unique conditions for ocean acidification research. We provide detailed measurements of the environmental parameters and carbonate system at the cave, comparing them with environmental and biological data from Scilla, a control site unaffected by vent activity. Moreover, the quantification of the gaseous components and dissociated ion concentrations allows a better characterization of the peculiar conditions of this hydrothermal vent, in order to evaluate the presence of $CO_2$ emissions and other compounds that might be associated with volcanic phenomena such as fluid and groundwater emissions, and to establish the main drivers contributing to the local decrease in pH. In addition to lowering pH levels, volcanic emissions may also be responsible for local reductions in temperature and salinity as a result of cold groundwater inputs, even though previous studies on *Caryophyllia inornata* (Caroselli et al., 2015) have shown that the growth and population dynamics of the species are not affected by temperature variations, supporting the interpretation that the observed differences between populations are mainly driven by the chemical effects of the vent. Characterization of the bubbling gas emissions showed that the local vent released almost pure $CO_2$ (98.7 % $CO_2$; Table 3), with a gas composition comparable to other volcanic vents (e.g., Bottaro islet vent system: 98–99 % $CO_2$, 0.3–0.6 % $H_2S$, 0.2–0.3 % $N_2$, 0.01–0.02 % $O_2$; Goffredo et al., 2014). Detected $HS^-$ concentrations were higher than the mean dissolved sulfide levels reported for the water column (≈0.000066 mg/L; Luther and Tsamakis, 1989). Thus, these concentrations are strictly related to hydrothermal activity and to $H_2S$ gaseous emissions, and they may be highly variable, producing peaks and fluctuations in $HS^-$ concentration. Since $HS^-$ is extremely unstable in oxic environments (Luther and Tsamakis, 1989), it is rapidly oxidized to $SO_4^{2-}$, whose concentrations in the cave were found to be comparable to typical seawater levels (2777.5 mg/L; Goffredo et al., 2014). The combination of volcanic emissions in and around the cave resulted in high $pCO_2$ and consistently low pH levels, reducing the availability of carbonate ions ($CO_3^{2-}$). The lower salinity further contributes to reduced aragonite saturation states (Ω) compared to those observed in the ambient seawater at Scilla. Unlike other studied volcanic vent system (e.g. Papua- New Guinea, Fabricius et al., 2011; Japan, Agostini et al., 2021; Italy, Goffredo et al., 2014), which typically exhibit gradients in environmental parameters, the $CO_2$ vent cave displayed consistent environmental and carbonate chemistry conditions across the three sampling sites (Table 1). The observed mean $pH_T$ and Ω match high emission IPCC scenarios for 2100 (SSP3–7.0 and SSP5–8.5 scenario; IPCC, 2023), which predict decreases in global average ocean $pH_T$ up to 7.68 and $\Omega_a$ up to 1.89 (Jiang et al., 2023), making this site a valuable and previously undescribed natural laboratory for studying the effects of natural $CO_2$ emissions (Fabricius et al., 2011).

The reliability of growth analyses using CT scans and sclerochronology as an alternative tool to field measurements through time has already been established in several studies conducted on *C. inornata* and other Mediterranean solitary corals (Goffredo et al., 2010; Caroselli et al., 2016). In the current study, *C. inornata* showed an exponential decrease in mean growth rate with age that allows mature corals to allocate available energetic resources towards physiological processes other than growth such as reproduction, sedimentation removal, maintenance, and competition (Goffredo et al., 2010). Like other organisms characterized by asymptotic growth (*B. europaea*, Caroselli et al., 2019; *A. calycularis* Teixidó et al., 2020), *C. inornata* tends to reach a maximum size ($L_\infty$; Table 3), that can be affected by environmental conditions (e.g. solar radiation, temperature; Caroselli et al., 2016).

In the current study, the growth parameters ($L_\infty$ and $k$) showed no significant differences with those of the Scilla population, which inhabits environments with ambient seawater conditions and is not exposed to volcanic influence (Table 3; Caroselli et al., 2016). Growth parameters (Table 3) also aligned with general asymptotic length and growth constant values for this species along Western Italian coasts ($L_\infty$ = 15.8, 95 % CI = 13.1–18.5; $k$ = 0.072, 95 % CI = 0.054–0.090; Caroselli et al., 2016). The stability in *C. inornata*'s growth rate under the influence of $CO_2$ vent emissions further supports the remarkable resilience of this species to varying environmental conditions (Caroselli et al., 2016). While the growth rate was consistent with that of populations not exposed to acidified environments, the *Caryophyllia inornata* population exhibited different demographic trait values compared to Scilla (Caroselli et al., 2016; Table 4). Life history theory suggests that organisms may develop different life strategies to optimize their fitness in response to changing environmental conditions and selective pressures (Pianka, 1970). Among reproductive strategies, r/K theory has been widely used to describe organism and population dynamics under different environmental conditions (Pianka, 1970). Unstable and variable environments tend to promote opportunistic strategies (r-species) characterized by high fecundity, short generation time, high mortality rates, quick turn-over, small size, and high dispersal potential (Pianka, 1970). Some scleractinian corals evolved mixed life strategies (Goffredo et al., 2010). *Balanophyllia elegans* presents an r-demographic model but a K-type reproduction; *B. europaea* shows a K-demographic model and an intermediate reproduction strategy; conversely, *L. pruvoti* has an intermediate demographic model and an r-reproductive strategy (Goffredo et al., 2010). In the present study, *C. inornata* living at low $pH_T$ and Ω showed a shift in local population dynamics towards an *r*-demographic strategy, as suggested by lower mean age and biomass distribution, smaller size, reduced turnover time, and a higher rate of mortality thus maintaining similar population abundance compared to populations living under ambient pH/Ω conditions, such as those at Scilla. Dynamic demographic strategies in response to acidified environments have been documented in natural populations of other Scleractinian corals to ensure the maintenance of the energetic supply required by biological processes (Teixidó et al., 2020). For instance, natural populations of the colonial, aphotoendosymbiotic coral *A. calycularis* at the $CO_2$ vents in Ischia exhibit smaller colonies with a reduced number of polyps, enabling the partitioning of available energy among fewer individuals and the maintenance of calcification rates despite suboptimal conditions (Teixidó et al., 2020). A different response is shown by the solitary photoendosymbiotic coral *B. europaea* at the Bottaro islet vent system, where decreasing pH leads to a reduced number of individuals and lower biomass per square meter, as well as decreased recruitment efficiency. This results in a progressive decline in the abundance of young individuals and, consequently, an increase in the mean age of the population (Caroselli et al., 2019). Moreover, under relatively low pH and suboptimal calcifying conditions, *B. europaea* shows reduced calcification and skeletal density, while maintaining linear extension rates, thereby reaching sexual maturity size and sustaining reproductive processes, which were not affected by exposure to $CO_2$ vents in transplanted corals (Caroselli et al., 2019). Like *B. europaea*, *C. inornata* is a solitary, gonochoric and brooding coral (Marchini et al., 2015). However, it also exhibits continuous production of agamic embryos, a process that can occur even below the size required for sexual maturity (Marchini et al., 2015). Since this process allows reproduction in young and small individuals, it may be prevalent in populations composed predominantly or entirely of immature polyps, such as those of *C. inornata* at the $CO_2$ vent cave. The ability to reproduce agamically without reaching the size for sexual maturity reduces mean age and biomass of the population but could facilitate the reallocation of polyps energetic resources to support

other life processes under conditions of low pH and low Ω. This response may suggest a different life strategy than previously observed response of the solitary photoendosymbiotic *B. europaea* where acidified conditions determine a reduction in recruitment efficiency, older population and reduce number of individuals (Caroselli et al., 2019). By the opposite, the acidified environment of the $CO_2$ vent cave seems to drive a shift in *C. inornata* populations towards an opportunistic r-strategy (low turnover time, high percentage of immature polyps and younger population, asexual reproduction), potentially optimizing the energetic allocation of polyps and guaranteeing the maintenance of the population abundance. Given that the demographic parameters derived from the population model have no associated uncertainty and could not be statistically tested, further investigation is required to support these hypotheses. Reproductive and genetic analyses will elucidate the role of agamic reproduction and the recruitment efficiency of the population, while studies on skeletal properties will evaluate the calcification responses of *C. inornata* to the local environmental conditions.

This characterization of the demography of an aphotoendosymbiotic solitary coral naturally living at $CO_2$ vents, compared to coral species with different growth forms (solitary or colonial) and trophic strategies (photosymbiotic and non-photosymbiotic) may contribute to understanding how coral species adopt different strategies to acclimate to ocean acidification and represent an example of how they can thrive under long-term exposure to acidified environments.

## 5. Conclusions

This research represents the first characterization of a newly discovered $CO_2$ vent cave and the demographic profiling of an aphotoendosymbiotic solitary coral naturally inhabiting a $CO_2$-rich gas environment. The submerged $CO_2$ vent cave at Basiluzzo Island represents a unique environment where local $CO_2$ emissions lead to reduced $pH_T$, $CO_3^{2-}$ and Ω values below the current Mediterranean Sea average, in line with predicted IPCC's SSP3–7.0 and SSP5–8.5 scenarios for the coming decades. Despite prolonged exposure to acidified conditions, *C. inornata* exhibited growth rates comparable to those of populations from unacidified environments. Conversely, *C. inornata* at the $CO_2$ vent cave displayed a population structure shifted towards *r*-strategy demographic traits, characterized by young individuals, high mortality rates, and low turnover time. These findings highlight the ability of this resilient solitary coral to sustain growth under acidified conditions while displaying demographic shifts, offering crucial insights into how aphotoendosymbiotic corals may respond to future climate-driven ocean acidification.

## Abbreviations

| | |
|---|---|
| $A_t$ | total alkalinity |
| $pH_T$ | pH total scale |
| $pCO_2$ | partial pressure of carbon dioxide |
| $HCO_3^-$ | bicarbonate ions |
| $CO_3^{2-}$ | carbonate ions |
| $CO_2$ | carbon dioxide |
| DIC | dissolved inorganic carbon |
| $\Omega_c$ | calcite saturation state |
| $\Omega_a$ | aragonite saturation state |
| $NO_2^-$ | nitrite |
| $NO_3^-$ | nitrate |
| $NH_4^+$ | ammonium |
| $PO_4^+$ | phosphate |
| $Si(OH)_4$ | silicate |
| $n_{CT}$ | collected corals dated by CT scans |
| $n_{Ph}$ | number of individuals from photoquadrats dataset |
| $L_\infty$ | asymptotic length |
| k | growth constant |
| $N_t$ | number of individuals in each age class |
| t | coral age |
| $R^2$ | stability |
| Z | instantaneous rate of mortality |

## CRediT authorship contribution statement

**Chiara Cassarino:** Writing – review & editing, Writing – original draft, Visualization, Validation, Investigation, Formal analysis, Data curation. **Arianna Mancuso:** Writing – review & editing, Validation, Resources, Investigation, Formal analysis, Data curation. **Fiorella Prada:** Writing – review & editing, Resources, Investigation. **Teresa Sani:** Resources, Investigation. **Silvia Dall'Ara:** Investigation. **Oscar Wallnoefer:** Investigation. **Chiara Marchini:** Investigation, Data curation. **Franco Tassi:** Writing – review & editing, Validation, Formal analysis, Data curation. **Alessandra Campanelli:** Writing – review & editing, Data curation. **Mauro Marini:** Writing – review & editing, Resources, Investigation. **Jörg U. Hammel:** Validation, Resources, Investigation. **Jaap A. Kaandorp:** Validation, Investigation. **Giuseppe Falini:** Funding acquisition, Conceptualization. **Zvy Dubinsky:** Funding acquisition, Conceptualization. **Erik Caroselli:** Writing – review & editing, Validation, Supervision, Software, Resources, Project administration, Methodology, Data curation, Conceptualization. **Stefano Goffredo:** Writing – review & editing, Validation, Supervision, Resources, Project administration, Methodology, Investigation, Funding acquisition, Data curation, Conceptualization.

## Declaration of competing interest

The authors declare that they have no financial or non-financial conflict of interests.

## Acknowledgements

The research leading to these results has received funding from: 1) the European Research Council under the European Union's Seventh Framework Programme (FP7/2007–2013)/ ERC grant agreement n° 249930—CoralWarm: Corals and global warming: the Mediterranean versus the Red Sea, 2) the National Recovery and Resilience Plan (NRRP), Mission 4 Component 2 Investment 1.4 - Call for tender No. 3138 of 16 December 2021, rectified by Decree n.3175 of 18 December 2021 of Italian Ministry of University and Research funded by the European Union – NextGenerationEU. Project code CN_00000033, Concession Decree No. 1034 of 17 June 2022 adopted by the Italian Ministry of University and Research, CUP J33C22001190001, Project title "National Biodiversity Future Center - NBFC". EC was supported by the ALMA IDEA STRAMICRO grant (University of Bologna). Francesco Sesso and Eolo Sub diving center assisted in the field. The Scientific Diving School collaborated with the underwater activities. The experiment complied with current Italian law.

## Appendix A. Supplementary data

Supplementary data to this article can be found online at https://doi.org/10.1016/j.scitotenv.2025.180858.

## Data availability

Datasets generated and analyzed during the current study are available from the corresponding author on reasonable request.

## References

Agostini, S., Harvey, B.P., Milazzo, M., Wada, S., Kon, K., Floc'h, N., Komatsu, K., Kuroyama, M., Hall-Spencer, J.M., 2021. Simplification, not "tropicalization", of temperate marine ecosystems under ocean warming and acidification. Glob. Chang. Biol. 27 (19), 4771–4784. https://doi.org/10.1111/gcb.15749.

Benjamini, Y., Hochberg, Y., 1995. Controlling the False Discovery Rate: A Practical and Powerful Approach to Multiple Testing. J. R. Stat. Soc. Ser. B Stat Methodol. 57 (1), 289–300. https://doi.org/10.1111/j.2517-6161.1995.tb02031.x.

Beverton, R., Holt, S., 1956. A review of methods for estimating mortality rates in fish populations, with special reference to sources of bias in catch sampling. Rapports et Proces-Verbaux Des Réunions. Conseil International Pour l'Éxploration de La Mer 140, 67–83.

Capaccioni, B., Tassi, F., Vaselli, O., Tedesco, D., Rossi, P.L., 2005. The November 2002 degassing event at Panarea Island (Italy): five months of geochemical monitoring. Ann. Geophys. 48 (4–5). https://doi.org/10.4401/ag-3231.

Caroselli, E., Gizzi, F., Prada, F., Marchini, C., Airi, V., Kaandorp, J., Falini, G., Dubinsky, Z., Goffredo, S., 2019. Low and variable pH decreases recruitment efficiency in populations of a temperate coral naturally present at a CO 2 vent. Limnol. Oceanogr. 64 (3), 1059–1069. https://doi.org/10.1002/lno.11097.

Caroselli, E., Nanni, V., Levy, O., Falini, G., Dubinsky, Z., Goffredo, S., 2015. Latitudinal variations in biometry and population density of a Mediterranean solitary coral. Limnol. Oceanogr. 60 (4), 1356–1370. https://doi.org/10.1002/lno.10100.

Caroselli, E., Ricci, F., Brambilla, V., Mattioli, G., Levy, O., Falini, G., Dubinsky, Z., Goffredo, S., 2016. Relationships between growth, population dynamics, and environmental parameters in the solitary non-zooxanthellate scleractinian coral Caryophyllia inornata along a latitudinal gradient in the Mediterranean Sea. Coral Reefs 35 (2), 507–519. https://doi.org/10.1007/s00338-015-1393-9.

IBM Corp. Released, 2021. IBM SPSS Statistics for Windows, Version 28.0. IBM Corp, Armonk, NY.

Dickson, A.G., Millero, F.J., 1987. A comparison of the equilibrium constants for the dissociation of carbonic acid in seawater media. Deep Sea Res Part A 34 (10), 1733–1743. https://doi.org/10.1016/0198-0149(87)90021-5.

Dishon, G., Grossowicz, M., Krom, M., Guy, G., Gruber, D.F., Tchernov, D., 2020. Evolutionary Traits that Enable Scleractinian Corals to Survive Mass Extinction Events. Sci. Rep. 10 (1), 3903. https://doi.org/10.1038/s41598-020-60605-2.

Dunn, O.J., 1964. Multiple Comparisons Using Rank Sums. Technometrics 6 (3), 241–252. https://doi.org/10.1080/00401706.1964.10490181.

Enochs, I.C., Manzello, D.P., Donham, E.M., Kolodziej, G., Okano, R., Johnston, L., Young, C., Iguel, J., Edwards, C.B., Fox, M.D., Valentino, L., Johnson, S., Benavente, D., Clark, S.J., Carlton, R., Burton, T., Eynaud, Y., Price, N.N., 2015. Shift from coral to macroalgae dominance on a volcanically acidified reef. Nat. Clim. Chang. 5 (12), 1083–1088. https://doi.org/10.1038/nclimate2758.

Fabricius, K.E., Langdon, C., Uthicke, S., Humphrey, C., Noonan, S., De'ath, G., Okazaki, R., Muehllehner, N., Glas, M.S., Lough, J.M., 2011. Losers and winners in coral reefs acclimatized to elevated carbon dioxide concentrations. Nat. Clim. Chang. 1 (3), 165–169. https://doi.org/10.1038/nclimate1122.

Feely, R., Jiang, L.-Q., Wanninkhof, R., Carter, B., Alin, S., Bednaršek, N., Cosca, C., 2023. Acidification of the global surface ocean: what we have learned from observations. Oceanography. https://doi.org/10.5670/oceanog.2023.222.

Feudale, L., Bolzon, G., Lazzari, P., Salon, S., Teruzzi, A., Di Biagio, V., Coidessa, G., Alvarez, E., Amadio, C., Cossarini, G., 2023. Mediterranean Sea Biogeochemical Analysis and Forecast (Copernicus Marine Service MED-Biogeochemistry, MedBFM4 system) (Version 2) [Data set]. Copernicus Marine Service. https://doi.org/10.25423/cmcc/medsea_analysisforecast_bgc_006_014_medbfm4.

Foo, S.A., Byrne, M., 2021. Forecasting impacts of ocean acidification on marine communities: Utilizing volcanic CO 2 vents as natural laboratories. Glob. Chang. Biol. 27 (10), 1995–1997. https://doi.org/10.1111/gcb.15528.

Goffredo, S., Caroselli, E., Mattioli, G., Zaccanti, F., 2010. Growth and population dynamic model for the non-zooxanthellate temperate solitary coral Leptopsammia pruvoti (Scleractinia, Dendrophylliidae). Mar. Biol. 157 (12), 2603–2612. https://doi.org/10.1007/s00227-010-1522-5.

Goffredo, S., Prada, F., Caroselli, E., Capaccioni, B., Zaccanti, F., Pasquini, L., Fantazzini, P., Fermani, S., Reggi, M., Levy, O., Fabricius, K.E., Dubinsky, Z., Falini, G., 2014. Biomineralization control related to population density under ocean acidification. Nat. Clim. Chang. 4 (7), 593–597. https://doi.org/10.1038/nclimate2241.

Grigg, R.W., 1984. Resource management of precious corals. Mar. Ecol. 5 (1), 57–74. https://doi.org/10.1111/j.1439-0485.1984.tb00307.x.

Hahn, S., Rodolfo-Metalpa, R., Griesshaber, E., Schmahl, W.W., Buhl, D., Hall-Spencer, J. M., Baggini, C., Fehr, K.T., Immenhauser, A., 2012. Marine bivalve shell geochemistry and ultrastructure from modern low pH environments: environmental effect versus experimental bias. Biogeosciences 9 (5), 1897–1914. https://doi.org/10.5194/bg-9-1897-2012.

Hassoun, A.E.R., Bantelman, A., Canu, D., Comeau, S., Galdies, C., Gattuso, J.-P., Giani, M., Grelaud, M., Hendriks, I.E., Ibello, V., Idrissi, M., Krasakopoulou, E., Shaltout, N., Solidoro, C., Swarzenski, P.W., Ziveri, P., 2022. Ocean acidification research in the Mediterranean Sea: Status, trends and next steps. Front. Mar. Sci. 9. https://doi.org/10.3389/fmars.2022.892670.

IPCC, 2023. Climate Change 2021 – The Physical Science Basis. Cambridge University Press. https://doi.org/10.1017/9781009157896.

Jiang, L., Dunne, J., Carter, B.R., Tjiputra, J.F., Terhaar, J., Sharp, J.D., Olsen, A., Alin, S., Bakker, D.C.E., Feely, R.A., Gattuso, J., Hogan, P., Ilyina, T., Lange, N., Lauvset, S.K., Lewis, E.R., Lovato, T., Palmieri, J., Santana-Falcón, Y., Ziehn, T., 2023. Global surface ocean acidification indicators from 1750 to 2100. J. Adv. Model. Earth Syst. 15 (3). https://doi.org/10.1029/2022MS003563.

Lewis, E., Wallace, D., Allison, L.J., 1998. Program developed for CO{sub 2} system calculations. https://doi.org/10.2172/639712.

Luther, G.W.III, Tsamakis, E., 1989. Concentration and form of dissolved sulfide in the oxic water column of the ocean. Marine Chemistry 27, 165–177. https://doi.org/10.1016/0304-4203(89)90046-7.

Marchini, C., Airi, V., Fontana, R., Tortorelli, G., Rocchi, M., Falini, G., Levy, O., Dubinsky, Z., Goffredo, S., 2015. Annual Reproductive Cycle and Unusual Embryogenesis of a Temperate Coral in the Mediterranean Sea. PLoS One 10 (10), e0141162. https://doi.org/10.1371/journal.pone.0141162.

Marchini, C., Tortorelli, G., Guidi, E., Airi, V., Falini, G., Dubinsky, Z., Goffredo, S., 2020. Reproduction of the Azooxanthellate Coral Caryophyllia inornata Is Not Affected by Temperature Along an 850 km Gradient on the Western Italian Coast. Front. Mar. Sci. 6. https://doi.org/10.3389/fmars.2019.00785.

Montegrossi, G., Tassi, F., Vaselli, O., Bidini, E., Minissale, A., 2006. A new, rapid and reliable method for the determination of reduced sulphur (S2−) species in natural water discharges. Appl. Geochem. 21 (5), 849–857. https://doi.org/10.1016/j.apgeochem.2006.02.007.

Parsons, T.R., Maita, Y., Lalli, C.M., 1984. A Manual of Chemical & Biological Methods for Seawater Analysis. Pergamon.

Pauly, D., 1984. Fish population dynamics in tropical waters: A manual for use with programmable calculators, 8. International center for living and aquatic resources management.

Pianka, E.R., 1970. On R- and K-Selection. Am. Nat. 104 (940), 593–597.

Posit team, 2023. RStudio: Integrated Development Environment for R. Posit Software, PBC, Boston, MA. Available at: http://www.posit.co/.

Potvin, C., Roff, D.A., 1993. Distribution-Free and Robust Statistical Methods: Viable Alternatives to Parametric Statistics. Ecology 74 (6), 1617–1628. https://doi.org/10.2307/1939920.

R Core Team, 2024. _R: A Language and Environment for Statistical Computing_. R Foundation for Statistical Computing, Vienna, Austria. https://www.R-project.org/.

Schindelin, J., Arganda-Carreras, I., Frise, E., Kaynig, V., Longair, M., Pietzsch, T., Cardona, A., 2012. Fiji: an open-source platform for biological-image analysis. Nat. Methods 9 (7), 676–682. https://doi.org/10.1038/nmeth.2019.

Sparre, P., Venema, S.C., 1989. Introduction to tropical fish stock assessment. Part I. Manual. FAO Fish. Tech. 1, 1–407.

Teixidó, N., Caroselli, E., Alliouane, S., Ceccarelli, C., Comeau, S., Gattuso, J., Fici, P., Micheli, F., Mirasole, A., Monismith, S.G., Munari, M., Palumbi, S.R., Sheets, E., Urbini, L., De Vittor, C., Goffredo, S., Gambi, M.C., 2020. Ocean acidification causes variable trait-shifts in a coral species. Glob. Chang. Biol. 26 (12), 6813–6830. https://doi.org/10.1111/gcb.15372.

The MathWorks Inc., 2022. MATLAB version: 9.13.0 (R2022b). The MathWorks Inc., Natick, Massachusetts. https://www.mathworks.com.

UCSanDiego, Scripps Institution of Oceanography, 2024. The Keeling Curve. Available at: https://keelingcurve.ucsd.edu. (Accessed 15 January 2025).

Uppström, L.R., 1974. The boron/chlorinity ratio of deep-sea water from the Pacific Ocean. Deep-Sea Res. Oceanogr. Abstr. 21 (2), 161–162. https://doi.org/10.1016/0011-7471(74)90074-6.

von Bertalanffy, L., 1938. A quantitative theory of organic growth (inquires on growth laws II). Hum. Biol. 10 (2), 181–213.

Vongsavat, V., Winotai, P., Meejoo, S., 2006. Phase transitions of natural corals monitored by ESR spectroscopy. Nucl. Instrum. Methods Phys. Res., Sect. B 243 (1), 167–173. https://doi.org/10.1016/j.nimb.2005.07.197.

Vuleta, S., Nakagawa, S., Ainsworth, T.D., 2024. The global significance of Scleractinian corals without photoendosymbiosis. Sci. Rep. 14 (1), 10161. https://doi.org/10.1038/s41598-024-60794-0.

Wilde, F., Ogurreck, M., Greving, I., Hammel, J.U., Beckmann, F., Hipp, A., Lottermoser, L., Khokhriakov, I., Lytaev, P., Dose, T., Burmester, H., Müller, M., Schreyer, A., 2016. Micro-CT at the imaging beamline P05 at PETRA III. AIP Conf. Proc., 030035 https://doi.org/10.1063/1.4952858.

Zibrowius, H., 1980. Les scléractiniaires de la Méditerranée et de l'Atlantique nord-oriental, 11. Institut océanographique.